Microelectronics Reliability 54 (2014) 1363–1368

Contents lists available at ScienceDirect

Microelectronics Reliability

journal homepage: www.elsevier.com/locate/microrel

Thermal stresses in a multilayered thin film thermoelectric structure

Z.-H. Jin *

Department of Mechanical Engineering, University of Maine, Orono, ME 04469, USA

ARTICLE INFO

Article history:
Received 1 October 2013
Received in revised form 16 February 2014
Accepted 26 February 2014
Available online 20 March 2014

ABSTRACT

This work investigates thermally induced stresses and deformations in a multilayered thin film thermoelectric (TE) structure for assessing thermomechanical reliability of the TE devices. The multilayered structure consists of a n-type and p-type thermocouple separated by an insulating layer, and an additional supporting membrane layer. The one-dimensional thermoelectricity is used to compute the temperature distribution with heat transfer by radiation and convection at the film surfaces being considered. The thermoelasticity theory of laminated composites is employed to determine the stresses and deformations in the thin film structure. It is found that the thermal stress calculated using the present laminate model has a significantly higher magnitude than that predicted by the strength of materials model. Effects of heat transfer coefficient at the film surfaces are also examined.

1. Introduction

Thermoelectric (TE) materials have been considered a promising material technology for converting waste heat to electric power. The energy conversion efficiency of TE materials is described by the so-called figure of merit $ZT = S^2T/\rho k$, where S is the Seebeck coefficient, ρ the electrical resistivity, k the thermal conductivity and T the temperature. Generally speaking, conventional TE devices have macroscopic dimensions and low figure of merit, which renders them inapplicable in microelectronics applications. In recent years, thin film thermoelectric materials for microelectronics applications have been developed with enhanced energy conversion efficiency represented by the increased figure of merit, see, for example, Rowe et al. [1], Volklein et al. [2], Venkatasubramanian et al. [3], Chen et al. [4], Bottner et al. [5,6], and Takashiri et al. [7].

Thermoelectrics are subjected to thermal gradients under operation conditions. The thermal gradient is produced by both the temperature difference applied at the hot and cold ends of the thermoelectric element and the Joule heating due to the thermoelectric effects. The thermal gradient induces thermal stresses which may cause failure of the thermoelectric structure. Assessment of thermomechanical reliability of thin film thermoelectric devices requires a thorough understanding of thermal stresses in the structures. Thermal stresses in thermoelectric thin films have been investigated by Huang et al. [8,9]. They computed the thermal stresses in a four-layered thermoelectric element using both a one-dimensional (1D) strength of materials model and a two-dimensional (2D) finite element numerical method, and concluded that the thermal stresses of the 1D and 2D models differ in the end regions of the structure. The 1D strength of materials model may be used to estimate the thermal stress in the preliminary design. Mahan [10], Volklein et al. [2], and Zabrocki et al. [11] also showed that the 1D model is appropriate in analyzing the temperature field in thermoelectrics. Jin [12] calculated the temperature that causes buckling failure of a thin film thermoelectric structure using the membrane force derived from the strength of materials model.

Multilayered thin film thermoelectric structures may have properties and configurations that are asymmetric about its geometrical mid-plane. More accurate determination of the stresses and deformations in the structure requires employment of laminated composites theories which have not been addressed in the literature to the author's best knowledge. This work presents an analytical model to compute the stresses and deformations in a multilayered thermoelectric structure using a theory of laminated composites. Because the length-to-thickness ratios of thin film thermoelectrics may reach an order of 1000 [2,13], the classical laminate theory may be appropriate for evaluating the thermal stresses and deformations in the structure. The remainder of this paper is organized as follows. Section 2 presents the basic equations of one-dimensional thermoelectricity and obtains the temperature field in a four-layer thin film structure consisting of a n-type and p-type thermocouple separated by an insulating layer, and an additional supporting membrane layer. Section 3 first describes the equations of the classical laminate theory for the multilayered thermoelectric structure and subsequently derives the equations for computing the thermal stresses and deformations. In Section 4, numerical results are presented to illustrate the differences between the predictions of the laminate model of this work

* Tel.: +1 (207)581 2135.
E-mail address: zhihe.jin@maine.edu

http://dx.doi.org/10.1016/j.microrel.2014.02.028
0026-2714/

and the strength of materials model. The effects of heat transfer at the film surfaces on the thermal stresses are also examined. Finally, conclusions are provided in Section 5.

2. Temperature field

Consider a multilayered thin-film thermoelectric (TE) structure as shown in Fig. 1. The structure is a four-layer TE element consisting of a n-type and p-type thermoelectric couple (layer #2 and #4), an insulating layer (layer #3) and a supporting membrane (layer #1). The structural configuration is the same as that studied by Huang et al. [8,9] which is an idealized model of the thermoelectric structure fabricated by Volklein et al. [2]. It is assumed that the two thermoelectric films have the same properties and thickness. Moreover, the insulating and supporting layers have the same thickness. The geometric mid-plane of the structure is thus the interface between the n-type and insulating layers. We note that layers of different thicknesses can be considered similarly as long as the geometric mid-plane of the structure is located at an interface between the layers. Furthermore, if the geometric mid-plane is not at an interface, the problem can still be treated by assuming the layer containing the geometric mid-plane as two layers of the same properties perfectly bonded along the geometric mid-plane.

Volklein et al. [2] and Huang et al. [8,9] analyzed the temperature distribution in the four-layer TE element assuming one-dimensional (1D) steady state heat flow in the longitudinal direction (x-direction). This section first summarizes the basic equations of 1D thermoelectricity and subsequently revisits the temperature field in the TE element using boundary conditions appropriate for TE generators. The temperatures at the cold and hot ends of the TE element are denoted by T_0 and T_h, respectively.

Consider 1D steady state electrical and heat conduction in the longitudinal direction (x-direction) of the thermoelectric structure. The basic equations for the thermoelectric films are [10,14]

$$q = -k_{pn}\frac{dT}{dx} + JST \tag{1}$$

$$\frac{dq}{dx} = JS\frac{dT}{dx} + \rho J^2 \tag{2}$$

$$\frac{dJ}{dx} = 0 \tag{3}$$

where T is the temperature, q the heat flux, J the electric current density, S the Seebeck coefficient, k_{pn} the thermal conductivity, and ρ the electrical resistivity. We assume that the n-type and p-type thermoelectric films have the same material properties. For the support and insulation layers, the term involving the electric current should be dropped in Eqs. (1) and (2). Clearly, the electric current density J is a constant in 1D steady state electrical conduction according to Eq. (3).

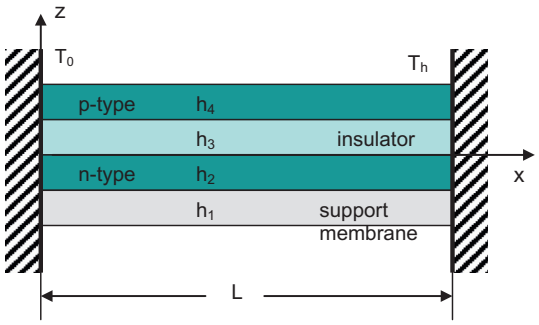

Fig. 1. A multilayered thin film thermoelectric element subjected to a temperature differential.

In deriving the governing equation of the temperature field, we adopt the approach of Volklein at el. [2] by using an effective heat transfer coefficient, η, to describe the combined heat transfer by convection and radiation at the film surfaces, i.e., the heat flux in the outward normal direction of the film surfaces, q_n, is proportional to the temperature difference between the film temperature and the ambient temperature. Mathematically, this condition is expressed as follows

$$q_n = \eta(T - T_0) \tag{4}$$

Here we assume that the ambient temperature is the same as that at the cold junction, T_0.

By considering energy balance for a small differential element in the longitudinal direction of the multilayered structure, we can get the governing equation of the temperature in the structure as follows

$$\tilde{k}\frac{d^2(T-T_0)}{dx^2} - \frac{\eta}{h_2}(T - T_0) = -\rho J^2 \tag{5}$$

where $\tilde{k}$ is an effective thermal conductivity defined by

$$\tilde{k} = k_{pn} + \frac{h_1}{2h_2}k_{su} + \frac{h_3}{2h_2}k_{is} \tag{6}$$

in which k_{is} and k_{su} are the thermal conductivities of the insulating and supporting layers, respectively, and h_i (i = 1, 2, 3) the thicknesses of the supporting membrane, the n-type thermoelectric film and the insulating layer, respectively. Note that $h_1 = h_3$ as assumed.

The solution of Eq. (5) under the boundary conditions at the cold and hot ends ($T = T_0$ at $x = 0$, and $T = T_h$ at $x = L$) can be obtained as follows

$$T - T_0 = A\exp(\lambda x) + B\exp(-\lambda x) + \frac{h_2}{\eta}\rho J^2 \tag{7}$$

where λ is a parameter given by

$$\lambda = \sqrt{\frac{\eta}{\tilde{k}h_2}} \tag{8}$$

and A and B are constants given by

$$\begin{aligned} A &= \frac{1}{\exp(\lambda L) - \exp(-\lambda L)}\left\{\Delta T - [1 - \exp(-\lambda L)]\frac{h_2}{\eta}\rho J^2\right\}, \\ B &= \frac{-1}{\exp(\lambda L) - \exp(-\lambda L)}\left\{\Delta T + [\exp(\lambda L) - 1]\frac{h_2}{\eta}\rho J^2\right\} \end{aligned} \tag{9}$$

in which L is the length of the layered structure and ΔT is the temperature difference between the hot and cold junctions, i.e., $\Delta T = T_h - T_0$.

3. Thermal stresses

The classical lamination theory of layered structures may be appropriate for evaluating the in-plane thermal stresses and deformations in thin film thermoelectric structures because the length-to-thickness ratios of thin film thermoelectrics may reach an order of 1000 [2,13]. In the laminate model, the displacements U, V and W in the x-, y- and z-directions, respectively, are given by [15,16]

$$\begin{aligned} U &= u(x,y) - z\frac{\partial w}{\partial x}, \\ V &= v(x,y) - z\frac{\partial w}{\partial y}, \\ W &= w(x,y) \end{aligned} \tag{10}$$

where $u(x,y)$ and $v(x,y)$ are the displacements of the geometrical mid-plane ($z = 0$) of the multilayered structure. As a first order

approximation, we assume that the displacements vary only in the longitudinal x-direction as the temperature T is only a function of x. This is the so called cylindrical bending which can accurately capture the normal thermal stress in the longitudinal direction that may cause compressive or buckling failure, one of major concerns in the design for thermomechanical reliability of the thin film structure. Another failure mode is delamination caused by the shear stresses between the neighboring layers of the TE structure [9]. Accurate determination of the shear stresses requires employment of general bending theory which will be addressed in the future study. Now the basic equations for the mid-plane displacements u, v and w (as functions of x only) reduce to [15,16]

$$A_{11}\frac{d^2u}{dx^2}-B_{11}\frac{d^3w}{dx^3}=\widehat{N}^T_{xx}\frac{d(T-T_0)}{dx} \tag{11a}$$

$$\frac{d^2v}{dx^2}=0 \tag{11b}$$

$$D_{11}\frac{d^4w}{dx^4}-B_{11}\frac{d^3u}{dx^3}=\widehat{M}^T_{xx}\frac{d^2(T-T_0)}{dx^2} \tag{11c}$$

The decoupled form of the above equations for u and w can be obtained as follows

$$\left(A_{11}-\frac{B_{11}^2}{D_{11}}\right)\frac{d^3u}{dx^3}=\left(\widehat{N}^T_{xx}+\frac{B_{11}}{D_{11}}\widehat{M}^T_{xx}\right)\frac{d^2(T-T_0)}{dx^2} \tag{12a}$$

$$\left(D_{11}-\frac{B_{11}^2}{A_{11}}\right)\frac{d^4w}{dx^4}=\left(\widehat{M}^T_{xx}+\frac{B_{11}}{A_{11}}\widehat{N}^T_{xx}\right)\frac{d^2(T-T_0)}{dx^2} \tag{12b}$$

where A_{11}, B_{11}, D_{11}, $\widehat{N}^T_{xx}$ and $\widehat{M}^T_{xx}$ are given by

$$\begin{aligned}A_{11}&=\sum_{k=1}^{4}\frac{E_k}{1-\nu_k^2}(z_k-z_{k-1}),\\ B_{11}&=\frac{1}{2}\sum_{k=1}^{4}\frac{E_k}{1-\nu_k^2}(z_k^2-z_{k-1}^2),\\ D_{11}&=\frac{1}{3}\sum_{k=1}^{4}\frac{E_k}{1-\nu_k^2}(z_k^3-z_{k-1}^3)\end{aligned} \tag{13}$$

$$\begin{aligned}\widehat{N}^T_{xx}&=\sum_{k=1}^{4}\frac{E_k\alpha_k}{1-\nu_k}(z_k-z_{k-1}),\\ \widehat{M}^T_{xx}&=\frac{1}{2}\sum_{k=1}^{4}\frac{E_k\alpha_k}{1-\nu_k}(z_k^2-z_{k-1}^2)\end{aligned} \tag{14}$$

in which E_k, ν_k and α_k are Young's modulus, Poisson's ratio and the coefficient of thermal expansion of the kth layer, respectively, and z_k are the z-coordinates of the plate surfaces and the interfaces between the layers defined by

$$\begin{aligned}z_0&=-(h_1+h_2),\\ z_1&=-h_2,\\ z_2&=0,\\ z_3&=h_3=h_2,\\ z_4&=h_3+h_4=h_1+h_2\end{aligned} \tag{15}$$

The boundary conditions for the displacement field are

$$\begin{aligned}&u=v=0,\quad \text{at } x=0,\ L\\ &w=0,\quad \frac{dw}{dx}=0,\quad \text{at } x=0,\ L\end{aligned} \tag{16}$$

for the clamped ends, and

$$\begin{aligned}&u=v=0,\quad \text{at } x=0,\ L\\ &w=0,\quad \frac{d^2w}{dx^2}=0,\quad \text{at } x=0,\ L\end{aligned} \tag{17}$$

for the pinned ends.

It follows from the basic Eq. (11b) and the boundary conditions for the displacement v in Eqs. (16) and (17) that $v=0$. Solving the boundary value problem described by Eqs. ((12), (16), (17)) for the mid-plane displacements u and w, we have

$$\left(A_{11}-\frac{B_{11}^2}{D_{11}}\right)u=\left(\widehat{N}^T_{xx}+\frac{B_{11}}{D_{11}}\widehat{M}^T_{xx}\right)\overline{T}+\frac{a_u}{2}x^2+b_ux \tag{18}$$

$$\left(D_{11}-\frac{B_{11}^2}{A_{11}}\right)w=\left(\widehat{M}^T_{xx}+\frac{B_{11}}{A_{11}}\widehat{N}^T_{xx}\right)\overline{\overline{T}}+\frac{a_w}{6}x^3+\frac{b_w}{2}x^2+c_wx+d_w \tag{19}$$

where $\overline{T}$ and $\overline{\overline{T}}$ are

$$\begin{aligned}\overline{T}&=\int_0^x(T-T_0)dx=\frac{A}{\lambda}[\exp(\lambda x)-1]+\frac{B}{\lambda}[1-\exp(-\lambda x)]+\frac{h_2}{\eta}\rho J^2x,\\ \overline{\overline{T}}&=\int_0^x\overline{T}dx=\frac{A}{\lambda}\left[\frac{\exp(\lambda x)-1}{\lambda}-x\right]+\frac{B}{\lambda}\left[x-\frac{1-\exp(-\lambda x)}{\lambda}\right]+\frac{h_2}{2\eta}\rho J^2x^2\end{aligned} \tag{20}$$

and the integration constants a_u, b_u, a_w, b_w, c_w and d_w are determined as follows

$$\begin{aligned}a_u&=\frac{B_{11}}{D_{11}}a_w,\\ b_uL^2&=-\left(\widehat{N}^T_{xx}+\frac{B_{11}}{D_{11}}\widehat{M}^T_{xx}\right)L\overline{T}(L)-3\frac{B_{11}}{D_{11}}\left(\widehat{M}^T_{xx}+\frac{B_{11}}{A_{11}}\widehat{N}^T_{xx}\right)[2\overline{\overline{T}}(L)-L\overline{T}(L)]\end{aligned} \tag{21a}$$

$$\begin{aligned}a_wL^3&=6\left(\widehat{M}^T_{xx}+\frac{B_{11}}{A_{11}}\widehat{N}^T_{xx}\right)[2\overline{\overline{T}}(L)-L\overline{T}(L)],\\ b_wL^2&=-2\left(\widehat{M}^T_{xx}+\frac{B_{11}}{A_{11}}\widehat{N}^T_{xx}\right)[3\overline{\overline{T}}(L)-L\overline{T}(L)]\end{aligned} \tag{21b}$$

$$c_w=d_w=0 \tag{21c}$$

for the clamped ends, and

$$\begin{aligned}a_u&=\frac{B_{11}}{D_{11}}a_w,\\ b_uL&=-\left(\widehat{N}^T_{xx}+\frac{B_{11}}{D_{11}}\widehat{M}^T_{xx}\right)\overline{T}(L)-\frac{L^2}{2}\frac{B_{11}}{D_{11}}a_w\end{aligned} \tag{22a}$$

$$a_w=-\left(\widehat{M}^T_{xx}+\frac{B_{11}}{A_{11}}\widehat{N}^T_{xx}\right)\frac{\Delta T}{L},\quad b_w=0 \tag{22b}$$

$$c_w=-\frac{a_w}{6}L^2,\quad d_w=0 \tag{22c}$$

for the pinned ends.

A major concern in the reliability design of thin film thermoelectrics is the normal stress in the longitudinal direction. The stress in the kth layer (k = 1, 2, 3, 4) is given by

$$\sigma_{xx}^{(k)}=\frac{E_k}{1-\nu_k^2}\left(\varepsilon^0_{xx}+z\kappa^0_{xx}\right)-\frac{E_k\alpha_k}{1-\nu_k}(T-T_0) \tag{23}$$

where the normal strain ε^0_{xx} and the curvature κ^0_{xx} of the mid-plane are

$$\left(A_{11}-\frac{B_{11}^2}{D_{11}}\right)\varepsilon^0_{xx}=\left(\widehat{N}^T_{xx}+\frac{B_{11}}{D_{11}}\widehat{M}^T_{xx}\right)(T-T_0)+a_ux+b_u \tag{24}$$

$$\left(D_{11}-\frac{B_{11}^2}{A_{11}}\right)\kappa_{xx}^0=-\left(\widehat{M}_{xx}^T+\frac{B_{11}}{A_{11}}\widehat{N}_{xx}^T\right)(T-T_0)-a_w x-b_w \tag{25}$$

Finally, the thermal stresses in the strength of materials model is given by [12]

$$\sigma_{xx}^{(k)}=E_k\varepsilon_{xx}^{(smm)}-E_k\alpha_k(T-T_0) \tag{26a}$$

where

$$\varepsilon_{xx}^{(smm)}=\left[\sum_{i=1}^{4}E_i\alpha_i h_i\Big/\sum_{i=1}^{4}E_i h_i\right]\left[(T-T_0)-\frac{\overline{T}(L)}{L}\right] \tag{26b}$$

Eqs. (23) and (26) show that the normal stress prediction of the laminate model differs from that of the strength of materials model by considering the Poisson's ratio effect, the curvature of the deformed thin film structure, and the extension-bending coupling effect on the normal strain. These differences are illustrated by the numerical examples in the following section.

4. Numerical results and discussion

In the numerical calculations, we use the material parameters listed in Table 1 [2,8]. The temperatures at the cold and hot ends are T_0 = 290 K and T_h = 330 K, respectively. The temperature dependence of the properties is not considered. All layers are assumed to have the same thickness, i.e., $h_1 = h_2 = h_3 = h_4$ = 1 μm, and the length is assumed to be L = 300 μm in the numerical examples. Finally, we use the following electrical current density that approximately corresponds to the peak conversion efficiency

$$J_{pk}=-\frac{k_{pn}\Delta T}{SL[T_h-(\Delta T/2)(k_{pn}/\tilde{k})]}\left(\sqrt{1+Z[T_h-(\Delta T/2)(k_{pn}/\tilde{k})]}-1\right) \tag{27}$$

where $Z = S^2/(\rho k_{pn})$ is the dimensional figure of merit.

Fig. 2 shows the thermal stress σ_{xx} in the longitudinal direction of the thin film structure with clamped ends. The Young's modulus of the insulating layer equals 75 GPa and the heat transfer at the film surfaces is not considered, i.e., η = 0. The thermal stresses in the p-type and n-type thermoelectric layers are about the same because the two films have the same material properties and the curvature effect is not significant (see Fig. 7) as indicated by Eq. (23). It is seen from the figure that the thermal stresses are compressive in the support membrane layer and the thermoelectric layer. The compressive stress in the support membrane increases from the cold end to its maximum of about 31 MPa at the hot end. The thermal stress in the n-type film, however, remains approximately flat over the length. Finally, the thermal stress in the insulating layer is compressive near the cold end and becomes tensile near the hot end.

Fig. 3 shows the thermal stress σ_{xx} in the multilayered structure using the strength of materials model as adopted in the existing studies [8,12]. All the material and geometrical properties are the same as those used in Fig. 2. The overall characteristics of the stress field are similar to those shown in Fig. 2. The magnitude of the stress in each layer, however, is much smaller. For example, the magnitude of the maximum compressive stress in the membrane is now 21 MPa which is about 2/3 of that using the more advanced laminate model shown in Fig. 2. Therefore, design of multilayered thin film thermoelectric structures for thermomechanical reliability should be based on the laminate model instead of the strength of materials model.

Table 1
Material properties.

	Thermoelectric films (n-type and p-type)	Insulating layer	Support layer
Young's modulus (GPa)	160	25, 75	138
Poisson's ratio	0.30	0.22	0.32
Coefficient of thermal expansion (10^6/K)	4.2	0.5	5.9
Thermal conductivity (W/(m K))	2.0	1.4	17.3
Electrical resistivity (Ω m)	0.6×10^{-5}		
Seebeck coefficient (μV/K)	200		

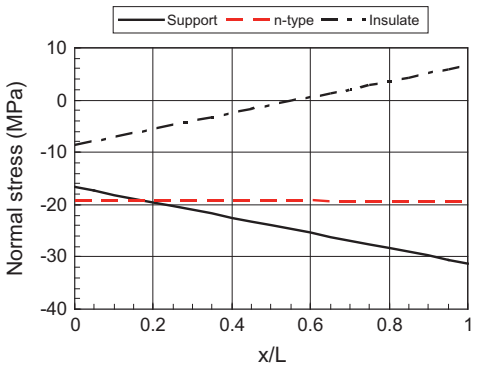

Fig. 2. Thermal stresses σ_{xx} in the longitudinal direction of the multilayered structure with clamped ends (Young's modulus of the insulating layer E_3 = 75 GPa, the effective heat transfer coefficient at the film surfaces η = 0).

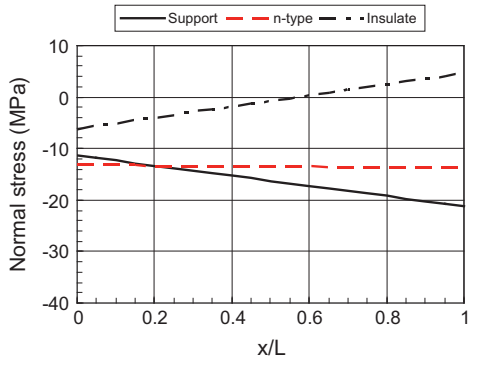

Fig. 3. Thermal stresses σ_{xx} in the longitudinal direction of the multilayered structure: strength of materials model (Young's modulus of the insulating layer E_3 = 75 GPa, the effective heat transfer coefficient at the film surfaces η = 0).

Fig. 4 shows the thermal stresses σ_{xx} in the multilayered structure with clamped ends. The Young's modulus of the insulating layer is now reduced to 25 GPa. All other material and geometrical properties are the same as those used in Fig. 2. Compared with the thermal stresses in the structure containing an insulating layer with a modulus of 75 GPa shown in Fig. 2, the thermal stress is reduced significantly in the insulating layer while deviates a little bit from those in other layers in Fig. 2. The implication is that the insulating layer may be designed as a non-load-bearing layer without significantly affecting the mechanical integrity of the overall structure.

The effect of heat transfer at the film surfaces on the thermal stresses in the thermoelectric structure is examined in Fig. 5 where only the stress in the supporting membrane is shown and the effective heat transfer coefficient at the film surfaces is assumed to be η = 20 J/(m^2 s K). It appears that consideration of surface heat transfer has an insignificant influence on the thermal stress particularly because the η value used in the calculation is probably larger than those encountered in practical designs.

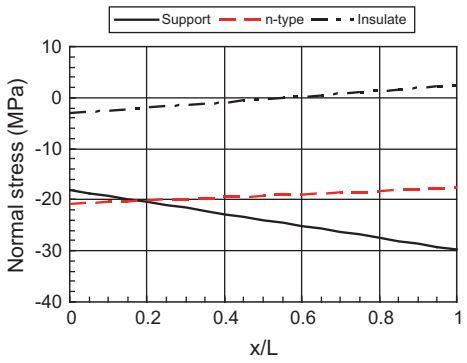

Fig. 4. Thermal stresses σ_{xx} in the longitudinal direction of the multilayered structure with clamped ends (Young's modulus of the insulating layer E_3 = 25 GPa, the effective heat transfer coefficient at the film surfaces η = 0).

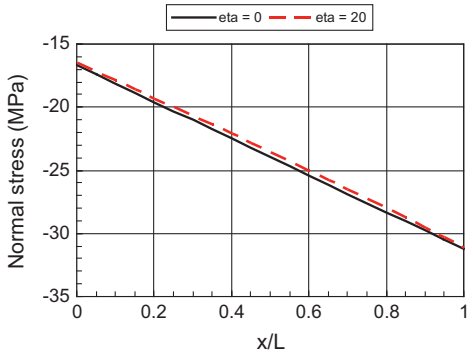

Fig. 5. Thermal stress σ_{xx} in the longitudinal direction of the membrane support layer in the structure with clamped ends (Young's modulus of the insulating layer E_3 = 75 GPa, the effective heat transfer coefficient at the film surfaces η = 0, 20).

To ascertain the effects of extension-bending coupling on the normal stress, we further examine the normal strain and curvature of the mid-plane of the multilayered structure with pinned ends because pinned ends result in a slightly larger deflection (out of plane displacement w). Fig. 6 compares the mid-plane normal strain ε^0_{xx} of the multilayered structure with the corresponding normal strain in the strength of materials model. All the material and geometrical properties are the same as those used in Fig. 4. It is seen that the maximum magnitude of the normal strain ε^0_{xx} of the laminate theory is about 25% higher than that of the strength of materials model.

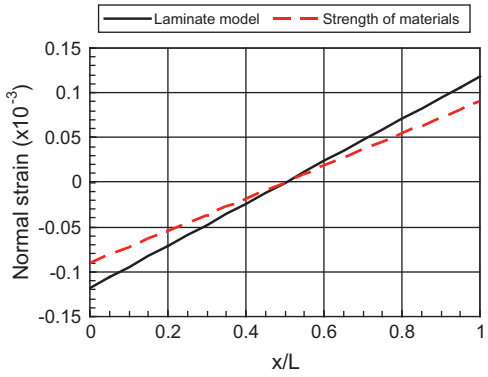

Fig. 6. Mid-plane normal strain ε^0_{xx} of the multilayered structure with pinned ends and the corresponding normal strain in the strength of materials model (Young's modulus of the insulating layer E_3 = 25 GPa, the effective heat transfer coefficient at the film surfaces η = 0).

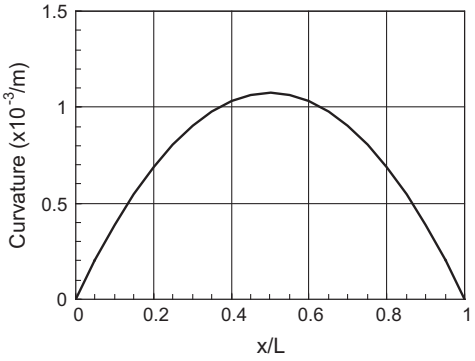

Fig. 7. Mid-plane curvature κ^0_{xx} of the multilayered structure with pinned ends (Young's modulus of the insulating layer E_3 = 25 GPa, the effective heat transfer coefficient at the film surfaces η = 0).

Fig. 7 shows the mid-plane curvature κ^0_{xx} of the multilayered structure with pinned ends. All the material and geometrical properties are the same as those used in Fig. 6. The curvature increases from zero at the ends of the film and reaches the peak at the mid-span of the structure. Although pronounced curvature is observed, its contribution to the normal stress is insignificant compared with that of the mid-plane normal strain because the coordinate z is on the order of a few microns, which shows that the extension-bending coupling influences the normal stress mostly through its effect on the normal strain.

5. Concluding remarks

Assessment of thermomechanical reliability of thin film thermoelectric devices requires a thorough understanding of thermal stresses in the devices because the thin film structures are subjected to sever thermal gradient under operation conditions. Knowledge of thermal stresses is also critical in predicting reliability and preventing failure of general microelectronic devices [17]. It has been known that compared with finite elements and other numerical methods, the strength of materials model is straightforward to implement and still provides reasonable results for design considerations. The laminate model presented in this work not only improves the predictions of the strength of materials approach but also remains as a convenient and feasible tool to evaluate thermal stresses and hence the structural integrity of thin film thermoelectric devices. The higher compressive normal stress compared with the strength of materials prediction will likely increase the probability of compressive failure of the semi-conductor thin-film structures. Moreover, buckling failure may also become possible for thin films with high length to thickness ratios under the increased compressive thermal stress.

We note that although the effects of extension-bending coupling and Poisson's ratio on the thermal stress are included in the present model, the cylindrical bending assumption does not consider variations of the field variables in the y-direction. Hence, a refined model that accounts for the y-dependence of the field variables should be employed in the future study. Furthermore, because the classical lamination theory assumes zero transverse shear strains, a higher order lamination theory (e.g., [18,19]) should be used to accurately determine the transverse shear strains and stresses which may cause delamination failure of multilayered thermoelectric structures.

Acknowledgements

This work is supported by the Maine Space Grant Consortium Research Infrastructure Seed Grant Program. The author would like

to thank Dr. X. Liu of IBM T.J. Watson Research Center for helpful discussions. The author would also like to thank four anonymous reviewers for their comments which greatly help improve the presentation of the paper.

References

[1] Rowe DM, Morgan DV, Keily JH. Miniature low-power/high-voltage thermoelectric generator. Electron Lett 1989;25:166–8.
[2] Volklein F, Min G, Rowe DM. Modeling of a microelectromechanical thermoelectric cooler. Sens Actuat A 1999;75:95–101.
[3] Venkatasubramanian R, Siivola E, Colpitts T, O'Quinn B. Thin-film thermoelectric devices with high room-temperature figures of merit. Nature 2001;413:597–602.
[4] Chen G, Dresselhaus MS, Dresselhaus G, Fleurial JP, Caillat T. Recent development in thermoelectric materials. Int Mater Rev 2003;48:45–66.
[5] Bottner H, Nurnus J, Gavrikov A, Kuhner G, Jagle M, Kunzel C, et al. New thermoelectric components using microsystem technologies. J Microelectromech Syst 2004;13:414–20.
[6] Bottner H, Chen G, Venkatasubramanian R. Aspects of thin-film superlattice thermoelectric materials, devices, and applications. MRS Bull 2006;31:211–7.
[7] Takashiri M, Tanaka S, Miyazaki K. Improved thermoelectric performance of highly-oriented nanocrystalline bismuth antimony telluride thin films. Thin Solid Films 2010;519:619–24.
[8] Huang MJ, Chou PK, Lin MC. Thermal and thermal stresses of a thin-film thermoelectric cooler under the influence of the Thomson effect. Sens Actuat A 2006;126:122–8.
[9] Huang MJ, Chou PK, Lin MC. An Investigation of the thermal stresses induced in a thin-film thermoelectric cooler. J Therm Stresses 2008;31:438–54.
[10] Mahan GD. Inhomogeneous thermoelectrics. J Appl Phys 1991;70:4551–4.
[11] Zabrocki K, Muller E, Seifert W. One-dimensional modeling of thermogenerator elements with linear material profiles. J Electron Mater 2010;39:1724–9.
[12] Jin ZH. Bulking of thin film thermoelectrics. Int J Fract 2013;180:129–36.
[13] Kwon SD, Ju BK, Yoon SJ, Kim JS. Fabrication of bismuth telluride based alloy thin film thermoelectric devices grown by metal organic chemical vapor deposition. J Electron Mater 2009;38:920–4.
[14] Jang B, Han S, Kim JY. Optimal design for micro-thermoelectric generator using finite element analysis. Microelectron Eng 2011;88:775–8.
[15] Hyer MW. Stress analysis of fiber-reinforced composite materials. updated ed. Lancaster, PA: DEStech Publications; 2009.
[16] Critescu ND, Cracium EM, Soos E. Mechanics of elastic composites. Boca Raton, Florida: Chapman & Hall/CRC; 2004.
[17] Suhir E. Could electronics reliability be predicted, quantified and assured? Microelectron Reliab 2013;53:925–36.
[18] Lo KH, Christensen RM, Wu EM. A higher-order theory of plate deformation – Part 2: laminated plates. ASME J Appl Mech 1977;44:669–76.
[19] Reddy JN. A simple higher-order theory for laminated composite plates. ASME J Appl Mech 1984;51:745–52.